Aarhus University

Master's Thesis

Beta-decay of 8Li: beta-alpha correlations and final state distribution

Author:
Anders Holst Rasmussen

Supervisor:
Hans O. U. Fynbo

June 8, 2021

Contents

1 Introduction

1.1 Motivation

When Henri Becquerel first discovered radioactivity in the 1890's, a new branch of atomic physics was born, namely nuclear physics, which is the study of the atomic nuclei, their constituents and interactions. Over the years it has evolved quickly, first by the discovery of three different types of radiation by Curie and Rutherford, to the discovery of different nucleons, that the nucleus itself is made of.

The technological advancements has made the study even more precise over the years, as the development of radioactive beams allow for the creation of specific short lived isotopes. This technique is known as Isotope Separation On-Line (ISOL), which was first developed in 1951 for the Copenhagen Cyclotron. Now the technology is available in many parts of the world, such as the IGISOL facility at the University of Jyväskylä in Finland. Another important advancement is the development of very precise detectors, such as the Double Sided Silicon Detector (DSSD), which allows for a very high energy and spacial resolution, which can give a detailed analysis of both coincidence and kinematics.

This brings us onto the current experiment that i have analyzed in this thesis. At the IGISOL facility, the experiment I257 was carried out in august 2020. The objective of the experiment was to measure β-decays from ^{8}Li and ^{12}B, however, this thesis will only govern the ^{8}Li decay.
The β-α angular correlation is previously shown with high precision to be nearly isotropic [1]. The study of the β-α correlation in ^{8}Li will therefore serve as a good indicator for the β-α correlation in ^{12}B, as the same setup

will be used for both experiment.
A former student has previously made an in depth analysis of the mirror nucleus ^{8}B, which can be used to compare the excitation energy of ^{8}Be. A comparison of the two is unfortunately out of scope for this thesis.

1.2 Nuclear decays

Lithium normally occurs stable as ^{6}Li and ^{7}Li, with the latter being the more abundant with 92.5% of all atoms. The longest living radioactive lithium isotope is ^{8}Li, with a half-life of 839 ms ref. When ^{8}Li decays, it will do so under a β-decay, immediately followed by the α-α breakup of an intermediate exited state in ^{8}Be, which has a half life of 1×10^{-16} s. ^{8}Be is a constituent in the triple-alpha process in stellar astrophysics, and creates a bottleneck for the creation of heavier elements, because of its very short lifespan.

1.2.1 β-decay

Most light unstable nuclei will decay by either proton/neutron emission, or by a β-decay. Isotopes that lie close to the valley of stability will not decay by proton/neutron emission, but from a β-decay.
A β-decay is a weak interaction, which allows a quark in a proton or neutron to change flavor, by emitting a W boson. This leads to the creation of either an electron/antineutrino pair or a positron/neutrino pair, shown as:

$$\beta^{+}: \quad p \rightarrow n + e^{+} + \nu_e \tag{1.1}$$

$$\beta^{-}: \quad n \rightarrow p + e^{-} + \bar{\nu_e}. \tag{1.2}$$

Nuclei below the valley of stability will decay by β^{-}, while nuclei above decays by β^{+}.
The energy for these decays are given by their Q-values, neglecting the very

small neutrino mass and the binding energy of the electrons gives:

$$Q_{\beta^+} = \left[m(^A_Z\mathrm{X}) - m(^A_{Z-1}\mathrm{X}')\right] c^2 \tag{1.3}$$

$$Q_{\beta^-} = \left[m(^A_Z\mathrm{X}) - m(^A_{Z+1}\mathrm{X}') - 2m_e\right] c^2, \tag{1.4}$$

where m is the mass of an atom with Z protons and A nucleons. The Q-values indicates the mass difference between the initial and final product., which can be either excitation energy or kinetic energy.
Not all β-decays are allowed. If the spin is unchanged, it is a Fermi transition, and if it changes it is a Gamow-Teller transition. An allowed decay is a transition with the orbital angular moment $L = 0$, and forbidden transitions is $L > 0$.
The nuclear part of the β-decay operator for an allowed decay is:

$$\mathcal{O}(\beta^\pm) = g_V \sum_A^{j=1} \tau_\mp(j) + g_A \sum_A^{j=1} \sigma(j)\tau_\mp(j), \tag{1.5}$$

where g_V is weak vector coupling constant, $\tau_\mp$ is the isospin step operator, g_A is the weak axial coupling constant and σ is the Pauli spin matrices. The first term corresponds to the Fermi operator, and the second term to the Gamow-Teller operator. This raises some selection rules, that dictate that for a Fermi decay, spin, isospin and parity must not be changed, and for a Gamow-Teller transitions, $\Delta J = 0, \pm 1$, $\Delta T = 0, \pm 1$, and $\Delta\pi = 0$.
The selection rules then enforces that not every energy level is populated in ^{8}Be.

1.2.2 α-decay

α-decay is another type of radioactive decay, where the nucleus emits an α-particle, and thereby decays into a different nucleus with the atomic number reduced by two. It has a Q-value of:

$$Q_\alpha = \left[m(^A_Z\mathrm{X}) - m(^{A-4}_{Z-2}\mathrm{X}') - m_\alpha\right] c^2. \tag{1.6}$$

Usually it is only elements heavier than nickel that can decay via this process, as the binding energy per nucleon decreases, and therefore becomes unstable towards spontaneous fission type processes. The only known exception to this rule is then ^{8}Be, which is the only light nuclei that decays by α-decay.

1.3 Structure of ^{8}Be

fig. 1.1 shows the excitation spectrum for ^{8}Be, with values from [2]. The spin, parity and isospin are written as $J^{\pi};T$ for each level. 4 different states has been shown for ^{8}Be, where only the first excited state is the broad state at 3.03 MeV. This state has conservation of spin and parity from ^{8}Li and is the only state that is allowed for the decay of ^{8}Li. Sittuated above is the broad state at 11.35 MeV, which does not conserve spin. Above that is a 16.626 MeV state, which conserves spin,parity and isospin, but lies energetically above ^{8}Li, so we would not expect that to shown in the data. It is still a quite relevant state, as the mirror nucleus ^{8}B $(2^{+};1)$ lies just above the energy at 17.979 MeV, and then has enough energy to populate this state, even though it is not very likely. Previous experiments made by the Aarhus subatomic group has examined the decay, and found only 5 counts populating this excitation level. But that should not show up when looking at the decay of ^{8}Li.

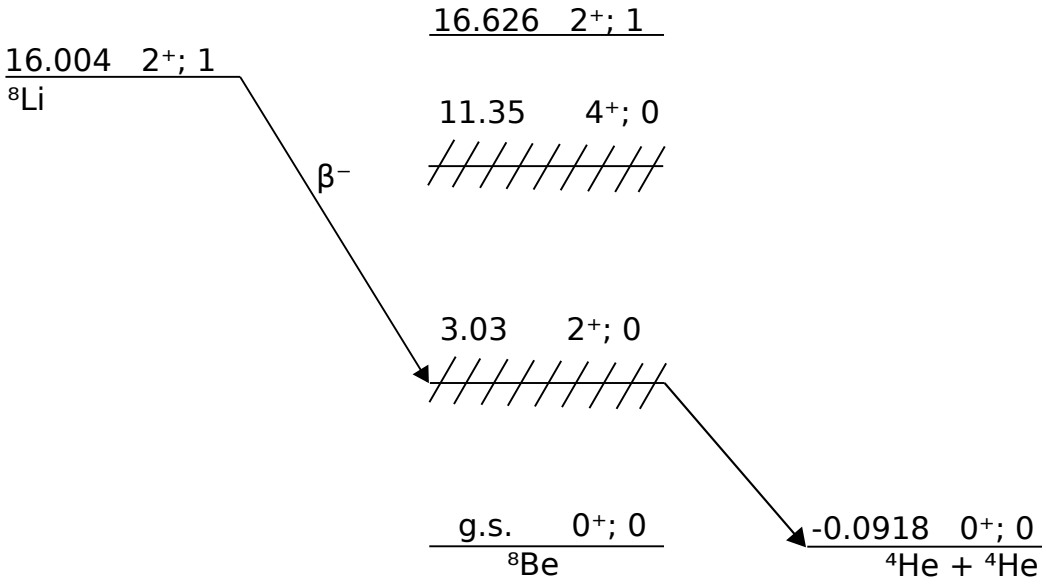

Figure 1.1: The decay scheme of ^{8}Li, and some notable excitation energies of ^{8}Be. Each level is labeld with the energy above the ^{8}Be ground state in MeV. Spin parity and isospin is noted as $J^{\pi};T$. All information is from [2].

2 Experimental Methods

The main goal of the experiment was to determine the β-α angular correlation. This was done at the IGISOL facility, at the University of Jyväskylä, where beams of all elements can be produced. The experiment took place in august 2020, due to a delay caused by the ongoing corona pandemic. This chapter will be concerning the experimental setup, a discussion of the detectors and an overview of the software used to extract and analyze the data.

2.1 Detector setup

The detection setup consists of 6 double sided silicon detectors (DSSD), and 6 single sided silicon detectors (SSD). The detectors are $5\,\mathrm{cm} \times 5\,\mathrm{cm}$ and placed in a cube around the a target in the center, as shown on figure fig. 2.2. The setup is designed with measuring the opening angle of the β in mind, and therefore the detectors covers 51% of the solid angle.

2.2 Experimental setup

The setup is designed to measure $\beta\alpha$ angular correlations in the β-delayed particle decay of ^{8}Li. When measuring multiple particles, the setup is highly dependent on the coverage of the solid angle. Therefore the setup is designed to have a large solid angle coverage, with high α-particle resolution, while still being able to measure β-particles.
This is has been achieved by creating a cube of six double sided silicon detectors (DSSD), all backed by a unsegmented silicon detectors (PAD). To gain the largest solid angle, the detectors where placed as close to one another as possible. A 3D printed case was designed to hold the detectors in place,

and achieved a solid angle coverage of 51% for the DSSD's, which can be seen on fig. 2.1. An illustration of the setup, together with the different detectors' thickness can be seen on fig. 2.2. Even though the setup was designed to hold 12 detectors in total, there where only 11 detectors in the actual experiment. The PAD behind Det1 was defect, and was therefore removed.

Detector	Thickness [μm]	PAD	Thickness[μm]
Det1	67	n/a	n/a
Det2	1002	P2	1036
Det3	65	P3	1497
Det4	60	P4	1490
DetU	60	PU	1498
DetD	1043	PD	1038

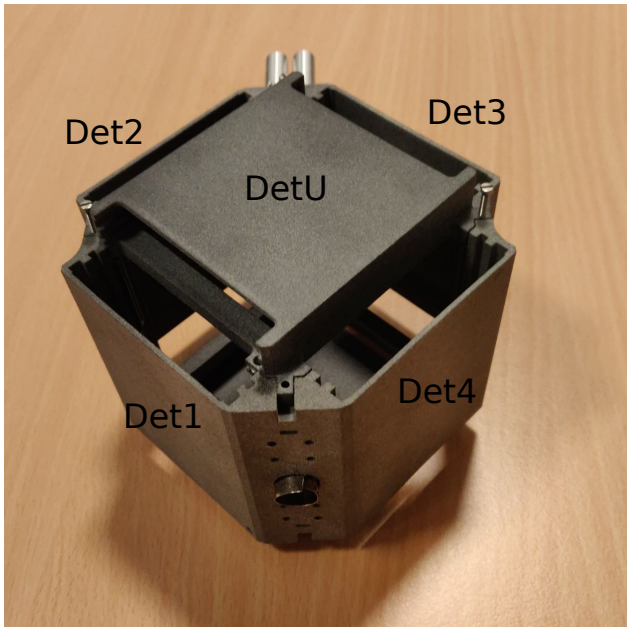

Figure 2.1: A picture of the 3D printed cube used to hold all detectors in place. The placement of the detectors have been shown, with exception of DetD, which was at the bottom of the cube. The beam enters the metal ring between Det1 and Det4

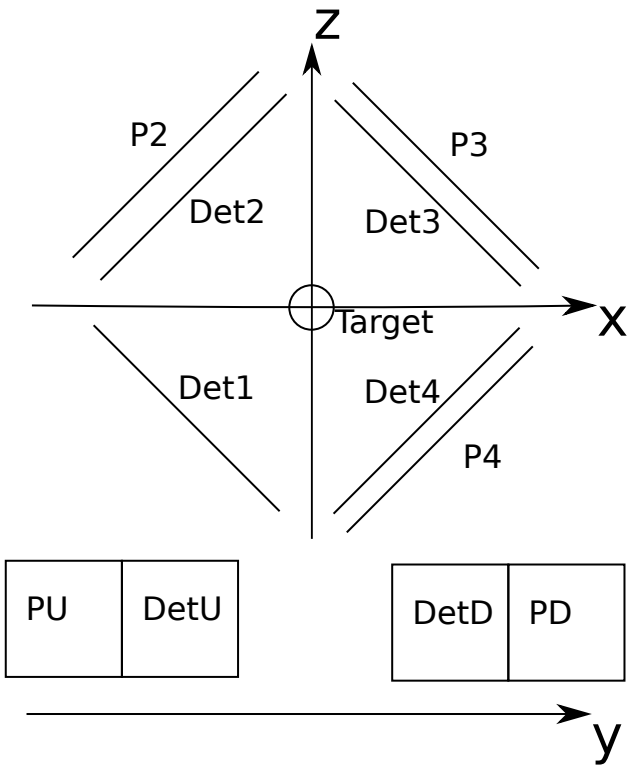

Figure 2.2: An illustration of the setup. Det1-Det4 are placed around the target, facing the target which is located at the center of the coordinate system. DetU are above the target, and DetD are below the target. Behind each detector is a PAD, with the exception of Det1, who's PAD was defect. The beam is parallel to the z-axis, entering the setup from the negative z-direction.

2.3 The detectors

As mentioned above, there where two types of detectors present in the setup. The first type is the Double sided silicon detector. As the name suggests, it consists of two sides, a front layer and a back layer. Each layer consists of 16 strips, that are placed in rows next to each other. The two layers are then arranged so each side are mutually orthogonal, which effectively makes pixels where each strip intersects a strip on the other side. An illustration of the detector can be seen on fig. 2.3.

The strips on the front side are p-doped, while the back side are n-doped.

When a charged particle hits the detector, it will ionize the atoms in the semi-conductor, and produce a electron-hole pair. The number of electron-hole pairs is proportional to the energy of the charged particle. The bias voltage on the detector collects the electrons and holes on opposite sites of the strip, where the charge is collected on aluminum contacts and a signal is measured. Energy is not deposited in these contacts, and therefore they constitute to a so called dead layer.
The detectors are square 5×5 cm and with their 16×16 strips, they have an effective gird of 256 pixels of 9 mm. 4 of the 6 detectors have a thickness of 60 μm and a dead layer of 100 nm dead layer. These detectors are the ones called Det1, Det3, Det4 and DetU in the setup seen on fig. 2.2. The other 2 detectors (Det2 and DetD) where both 1000 μm.

The other type of detector was the PADs. They are different from the DSSD's, in that they do not have sides, and no strips. Therefore they do not contain a grid, the same way the DSSD's do, and will not provide any information as to where a particle has hit. But they are included in the setup to detect excess energy of particles not stopped by the DSSD. This makes them good at detecting β-particles, as they will not be stopped by a DSSD. An α-particle will deposit all of its energy into the first DSSD it encoutner, and be effectively stopped completely by it, and a a β-particle will deposit almost no energy in a thin DSSD, and travel through it, ending up depositing some energy in the PAD.
Therefore one can roughly distinguish the α-particles from the β-particles, by observing whether a particle has hit the DSSD and the PAD.

Since there are also two thick DSSD's in the setup, one can also get some information from a β-particle from these thicker detectors, as it will deposit more energy in these detectors.

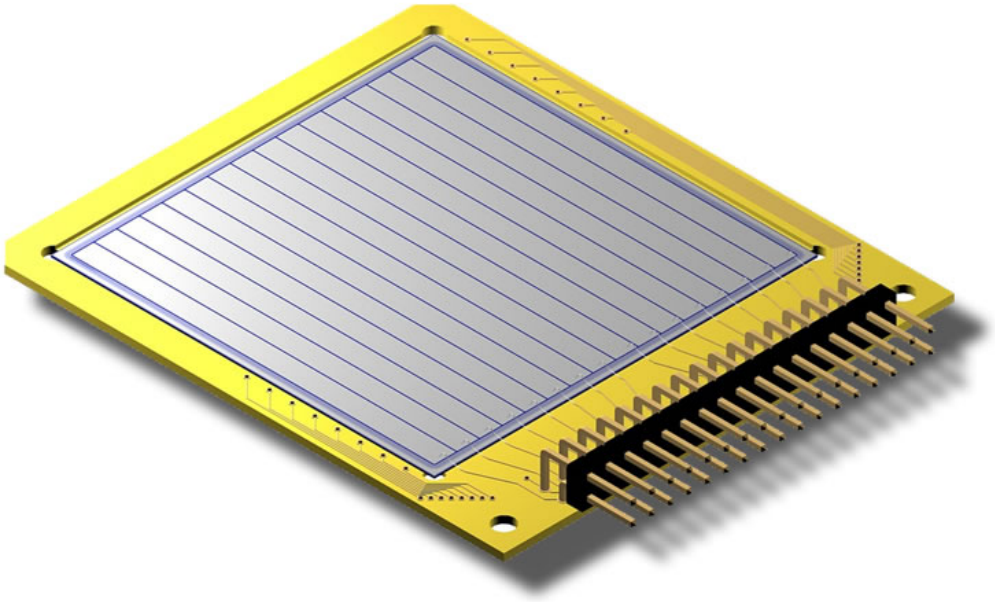

Figure 2.3: An illustration of the DSSD type used in this experiment. The detector has 16 p-doped strips, and 16 n-doped strips perpendicular to these. This gives 256 pixels for the detector. Image courtesy of Micron Semiconductor Ltd

2.4 AUSAlib and ROOT

ROOT [3] is an object oriented C++ framework that is designed primarily for data analysis in high-energy and nuclear physics. It was created at CERN in 1995, and has since grown and become the dominant analysis software at both CERN and many other nuclear and particle physics laboratories. ROOT was designed to handle large amounts of data with high computing efficiency.

ROOT makes an intelligent data structure by creating a "Tree" with the class `TTree`. This tree will then have "branches" which corresponds to some variable of the given detection event, such as the energy of the front strip or identity of the detector. This TTree then allows for reading of an individual

branch, while ROOT takes care of the memory management. One can also store a TTree to the disk in the form a .root file.

ASUALib [4] is a tool that build on top of ROOT. It was created by the subatomic group at Aarhus University. Before this tool was created, everyone in the group had to more or less create their own tools to get data from the detectors into a useful data structure. This meant that a lot of time was wasted just trying to access data from experiments. AUSAlib was therefore created, so the basic tasks of data extraction was automated.
AUSAlib has a lot of functionalities, but the two main tools that was used to extract data was the *Sorter* and *Calibrator*.

2.4.1 Unpacker

The `Unpacker` converts raw data from the detectors into a ROOT TTree. This is done by using the unpacking program `ucesb` [5]. This will setup the branch structure of the data. Some of these branches are `FT` and `BT`, which is a vector of the `TDC` (time) values for each event, for the front and backside of the detector. They are vectors because they contain information for each particle hits in a given time slot, for which there can be multiple. There are also the branches `FE` and `BE`, which is the `ADC` (energy) associated with the events.

2.4.2 Calibrator

Since the detectors work, by measuring an electrical charge that comes from the charged particle, the detectors needs to translate a specific charge to energy deposited.
To do that, we use the `Calibrator`-tool, which is designed to convert a channel number into an actual energy. Assuming that the channel numbers are linearly related to the energies, a known radioactive source can be measured, and the expected spectrum can be compared to the measured. This is done for each strip in each detector.

The `Calibrator` starts by running a peak-finding algorithm over some calibration data, to roughly identify the locations of the peaks, followed by a multi-Gaussian fit to find the most precise peak location. The positions of the peaks can then be compared to the expected energies, giving an associated energy to a given channel.

As mentioned earlier, all of the detectors have a small aluminum dead layer. All particles that pass through this layer will loses some amount of energy depending on the stopping power of the material and the effective thickness of the dead layer Δx_{eff}, which furthermore depends on the angle of incidence, θ. The relationship between the effective thickness and the actual thickness is described as $\Delta x_{eff} = \Delta x / \cos(\theta)$. This gives the measured energy as

$$E' = E - \frac{dE}{dx}\frac{\Delta x}{\cos(\theta)},$$

where E is the original energy of the particle, dE/dx is the stopping power of the material and Δx is the thickness of the dead layer. The stopping power is calculated from SRIM [6]

These calculations are all handled by the `Calibrator`. As input it takes an unpacked measurement of a source, a file specifying the locations of the expected peaks and a file specifying the spacial locations of the detectors. From this it calculates the energy loss, and creates a linear relationship between channel numbers and energies. This is then written to the disk as a seperate calibration file, which can be parsed to other modules.
It is important to note that the Calibrator does not modify any data. Therefore the energy loss is unaccounted for. Instead it corrects the expected energy spectrum, which means that the resulting calibration is still valid. The energy loss correction is therefore still needed in the analysis, as the effect is unaccounted for in measurements.

2.4.3 Sorter

The sorter is used after a successful calibration. It generates a ROOT file based on the unpacked data, and applies the calibration. It is also responsible for matching and combining events from the front-side to the back-side of the detector. If there where one hit in the front side and one in the back, the mathcing is fairly trivial. If there however where multiple hits in both front and back, the `Sorter` will run a matching algorithm, which pairs the hits with the lowest energy differences.

When the events have been matched, the hits on the individual sides of each detector are merged into a single event. Therefore each event can now be considered a multiple of particle hits. This makes it possible to to associate physical properties with each particle, such as direction and energy. There has still not been done any filtering of the data, which is what we will discuss in **??**.

Bibliography

[1] R. E. Tribble and G. T. Garvey. Induced weak currents and $\beta^{\pm} - \alpha$ angular correlations in $a = 8$. *Phys. Rev. C*, 12:967–983, Sep 1975.

[2] D.R. Tilley, J.H. Kelley, J.L. Godwin, D.J. Millener, J.E. Purcell, C.G. Sheu, and H.R. Weller. Energy levels of light nuclei a=8,9,10. *Nuclear Physics A*, 745(3):155–362, 2004.

[3] CERN. ROOT. https://root.cern/. 2021.

[4] M. Munch, J. Halkjær, and O. S. Kirsebom. Ausalib - aarhus subatomic library. https://git.kern.phys.au.dk/ausa/ausalib/wikis/home, 2017.

[5] ucesb. fy.chalmers.se/~f96hajo/ucesb/. Accessed June 8, 2021.

[6] James F. Ziegler, M.D. Ziegler, and J.P. Biersack. Srim – the stopping and range of ions in matter (2010). *Nuclear Instruments and Methods in Physics Research Section B: Beam Interactions with Materials and Atoms*, 268(11):1818–1823, 2010. 19th International Conference on Ion Beam Analysis.